Tafazzin deficiency impairs CoA-dependent oxidative metabolism in cardiac mitochondria

Received for publication, September 26, 2019, and in revised form, July 7, 2020 Published, Papers in Press, July 14, 2020, DOI 10.1074/jbc.RA119.011229

Catherine H. Le[1], Lindsay G. Benage[2], Kalyn S. Specht[3], Lance C. Li Puma[3], Christopher M. Mulligan[4], Adam L. Heuberger[5], Jessica E. Prenni[5], Steven M. Claypool[6], Kathryn C. Chatfield[7], Genevieve C. Sparagna[8], and Adam J. Chicco[1,3,4,*]

From the [1]Cell and Molecular Biology Program and the Departments of [2]Biochemistry and Molecular Biology, [3]Biomedical Sciences, [4]Food Science and Human Nutrition, and [5]Horticulture and Landscape Architecture, Colorado State University, Fort Collins, Colorado, USA, the [6]Department of Physiology, Johns Hopkins University School of Medicine, Baltimore, Maryland, USA, the [7]Department of Pediatrics, University of Colorado School of Medicine, Children's Hospital Colorado, Aurora, Colorado, USA, and the [8]Division of Cardiology, Department of Medicine, University of Colorado Anschutz Medical Campus, Aurora, Colorado, USA

Edited by Jeffrey E. Pessin

Barth syndrome is a mitochondrial myopathy resulting from mutations in the tafazzin (*TAZ*) gene encoding a phospholipid transacylase required for cardiolipin remodeling. Cardiolipin is a phospholipid of the inner mitochondrial membrane essential for the function of numerous mitochondrial proteins and processes. However, it is unclear how tafazzin deficiency impacts cardiac mitochondrial metabolism. To address this question while avoiding confounding effects of cardiomyopathy on mitochondrial phenotype, we utilized *Taz*-shRNA knockdown (Taz^{KD}) mice, which exhibit defective cardiolipin remodeling and respiratory supercomplex instability characteristic of human Barth syndrome but normal cardiac function into adulthood. Consistent with previous reports from other models, mitochondrial H_2O_2 emission and oxidative damage were greater in Taz^{KD} than in wild-type (WT) hearts, but there were no differences in oxidative phosphorylation coupling efficiency or membrane potential. Fatty acid and pyruvate oxidation capacities were 40–60% lower in Taz^{KD} mitochondria, but an up-regulation of glutamate oxidation supported respiration rates approximating those with pyruvate and palmitoylcarnitine in WT. Deficiencies in mitochondrial CoA and shifts in the cardiac acyl-CoA profile paralleled changes in fatty acid oxidation enzymes and acyl-CoA thioesterases, suggesting limitations of CoA availability or "trapping" in Taz^{KD} mitochondrial metabolism. Incubation of Taz^{KD} mitochondria with exogenous CoA partially rescued pyruvate and palmitoylcarnitine oxidation capacities, implicating dysregulation of CoA-dependent intermediary metabolism rather than respiratory chain defects in the bioenergetic impacts of tafazzin deficiency. These findings support links among cardiolipin abnormalities, respiratory supercomplex instability, and mitochondrial oxidant production and shed new light on the distinct metabolic consequences of tafazzin deficiency in the mammalian heart.

Barth syndrome (3-methylglutaconic aciduria type II; BTHS) is an X-linked mitochondrial disorder that results from loss-of-function mutations in the tafazzin gene (*TAZ*), leading to debilitating cardioskeletal myopathy, growth retardation, and neutropenia (1, 2). Tafazzin is a phospholipid transacylase responsible for the acyl-chain remodeling of cardiolipin (CL), a dimeric tetra-acyl phospholipid localized almost exclusively in the inner mitochondrial membrane. Cardiolipin is essential for maintaining the structural and functional integrity of many inner membrane proteins, including the electron transfer complexes (3–5), and their assembly into higher-order supercomplexes (6). In the healthy mammalian heart, the majority of cardiolipin acyl-chains are linoleic acid (18:2*n*6), and tetra-linoleoyl cardiolipin (L_4CL) is the predominant molecular species (7). Linoleoyl enrichment is achieved by acyl-chain exchange reactions with adjacent monomeric phospholipids catalyzed by tafazzin (8, 9), which enhances inner membrane stability by facilitating CL interaction with inner membrane proteins (10).

Loss of tafazzin function in the heart results in depletion of L_4CL, with an accumulation of nascent cardiolipin species containing more saturated acyl-chains and monolysocardiolipins (11–13). This abnormal cardiolipin profile is associated with destabilization of respiratory enzyme supercomplexes, reduced respiratory enzyme capacities, and increased generation of reactive oxygen species in BTHS patient–derived cell lines (14–19). Similar alterations are seen in mice with tafazzin deficiency (20, 21), but the nature and extent of mitochondrial defects varies across tissues, and respiratory impairment appears to depend on the substrate provided (21, 22). This suggests that adaptive responses to tafazzin deficiency *in vivo* may contribute to a more complex metabolic phenotype than can be revealed by cell model systems, which may be relevant to the pathogenesis and treatment of BTHS in humans.

The most severe clinical manifestation of BTHS is cardiomyopathy, which can present in infants or develop later in adulthood, despite persistent cardiolipin abnormalities beginning early in life (23). This phenotypic heterogeneity suggests that variations in tafazzin function or compensatory adaptations that preserve cardiac function must occur across affected individuals and highlights an incomplete understanding of how cardiolipin abnormalities impact the heart. To investigate the effects of tafazzin deficiency on the mammalian heart, an inducible *Taz* short hairpin RNA (shRNA) knockdown mouse

This article contains supporting information.

* For correspondence: Adam J. Chicco, adam.chicco@colostate.edu.

was developed to overcome the embryonic lethality of full genetic ablation (24, 25). Aggressive induction of *Taz* shRNA during gestation markedly impairs cardiac development, leading to fetal or neonatal noncompaction cardiomyopathy and early lethality (26), consistent with the most severe BTHS cases (27). However, lower doxycycline dosing during gestation produces offspring that live well into adulthood despite ~90% *Taz* deficiency and characteristic abnormalities in cardiolipin composition and mitochondrial morphology (24, 25). These mice exhibit exercise intolerance and growth delay consistent with human BTHS but maintain relatively normal cardiac function until ~6–7 months of age (24, 25, 28) despite impairments in cardiac mitochondrial function evident by 2–3 months of age (20–22, 28).

Understanding how tafazzin-deficient mice preserve basal cardiac function despite persistent cardiolipin abnormalities and respiratory chain defects could reveal novel strategies for attenuating the development of cardiomyopathy in BTHS. These mice also provide an ideal model for resolving the impact of aberrant cardiolipin remodeling on cardiac mitochondrial function without the confounding influence of cardiomyopathy. Therefore, the aim of this study was to define the cardiac mitochondrial phenotype of *Taz* shRNA mice through an integration of functional studies, cardiac metabolite analyses, and mitochondrial proteomic profiling, with a particular focus on elucidating the mechanism of substrate-specific respiratory impairment and identifying compensatory adaptations that manifest prior to the development of cardiac dysfunction.

Results

Taz-deficient mice maintain normal cardiac function despite cardiolipin defects and mitochondrial supercomplex instability

Doxycycline-inducible *Taz* shRNA mice originally generated on a C57Bl/6 background at TaconicArtemis, GmbH (Köln, Germany) were obtained from Dr. Zaza Khuchua (University of Cincinnati) (24) and used to establish a colony of tafazzin-deficient (Taz^{KD}) mice at Colorado State University for these studies. As described previously (24, 28), transgenic males were mated with WT (C57Bl/6) females to generate Taz^{KD} and WT littermate mice. The offspring were genotyped by PCR analysis of tail DNA for the presence of the 381-bp *Taz* shRNA gene product (Fig. S1*A*). All mice were maintained on Purina RMH1500 chow (Gray Summit, MO) supplemented with 625 ppm doxycycline to induce *Taz* shRNA expression in transgenic mice (24, 25) and control for any unintended effects of doxycycline in WT mice (29). The extent of tafazzin mRNA knockdown was >95% as previously reported (24) and was confirmed at the protein level in cardiac mitochondria by immunoblot detecting the expected ~25–34-kDa tafazzin protein bands in WT, but not Taz^{KD} (Fig. 1*A* and Fig. S1*B*). The body weights of adult mice were persistently lower in Taz^{KD} (25.8 ± 0.6 g) compared with WT mice (34.0 ± 1.3 g; $p < 0.01$), consistent with growth delay and small stature in this model and BTHS patients (24).

Male Taz^{KD} and WT littermates were studied at 4–6 months of age, when cardiolipin abnormities are well-established but before the onset of cardiac dysfunction (21, 24, 25). To confirm this, electrospray ionization Mass spectrometry was performed on cardiac mitochondrial phospholipids, which demonstrated expected losses of total CL and L_4CL with accumulation of monolysocardiolipin in Taz^{KD} *versus* WT mice within this age range (Fig. S1, *C–E*). Similarly, gas chromatographic analysis of fatty acids present in the cardiolipin fraction isolated by normal phase liquid chromatography revealed a predominant loss of linoleic acid with higher monounsaturated and saturated fatty acids in Taz^{KD} *versus* WT mitochondria, reflective of abundant nascent (nonremodeled) cardiolipin species (Fig. 1*B*). Interestingly, significant changes were also observed in the acyl composition of mitochondrial phosphatidylcholine and phosphatidylethanolamine (Fig. S1, *F* and *G*) and the total phospholipid fraction (Fig. 1*C*), consistent with broader effects of tafazzin deficiency on mitochondrial membrane composition than cardiolipin (22). Phospholipid compositional changes were nearly identical between subsarcolemmal (SS) and intermyofibrillar (IF) mitochondria, indicating similar effects of tafazzin deficiency in these major cardiac mitochondrial subpopulations.

Loss of linoleic acid in cardiolipin is thought to disrupt its interaction with membrane proteins (10), favoring a destabilization of mitochondrial supercomplexes that has been reported in BTHS patient cells (14, 30). Consistent with previous reports (19–21), cardiac mitochondria from Taz^{KD} mice used in the present study exhibited lower levels of high-molecular-mass protein bands associated with CI–CIII–CIV supercomplexes separated by blue native–PAGE, which were confirmed to contain lower levels of CI and CIII subunits by subsequent SDS-PAGE and immunoblotting (Fig. 1*D* and Fig. S2). Smaller-molecular-mass CIII–CIV complexes were unaffected, as recently reported in BTHS patient–derived fibroblasts (30), whereas the succinate dehydrogenase (CII) complex was significantly lower in Taz^{KD} *versus* WT (Fig. 1*D* and Fig. S2, *band 5*), consistent with the findings of Dudek *et al.* (21). Despite these defects, heart mass (142 ± 9 in Taz^{KD} and 149 ± 4 mg in WT) and contractile function (Fig. 1*E*) were similar in Taz^{KD} and WT mice through at least 6 months of age, consistent with previous reports using the same doxycycline dosing regimen (24). Taken together, these studies validate the utility of this Taz^{KD} mouse model for defining the impact of impaired cardiolipin remodeling and supercomplex instability on cardiac mitochondrial function in the absence of confounding cardiomyopathy.

Substrate-specific impairment of OXPHOS capacity in Taz-deficient cardiac mitochondria

Previous studies have produced variable evidence of mitochondrial respiratory enzyme dysfunction in BTHS patient–derived cells and Taz^{KD} mice depending on the experimental approach and substrates employed (18, 21, 22), highlighting an incomplete understanding of how tafazzin deficiency impacts cardiac mitochondrial function. To address this, we performed a comprehensive analysis of cardiac mitochondrial bioenergetics using isolated organelles and permeabilized left ventricular fibers (Fig. 2). Mitochondrial protein yield and subpopulation distributions from cardiac tissue were similar between Taz^{KD} and WT (Fig. 2*A*). Enzymatic activities of respiratory

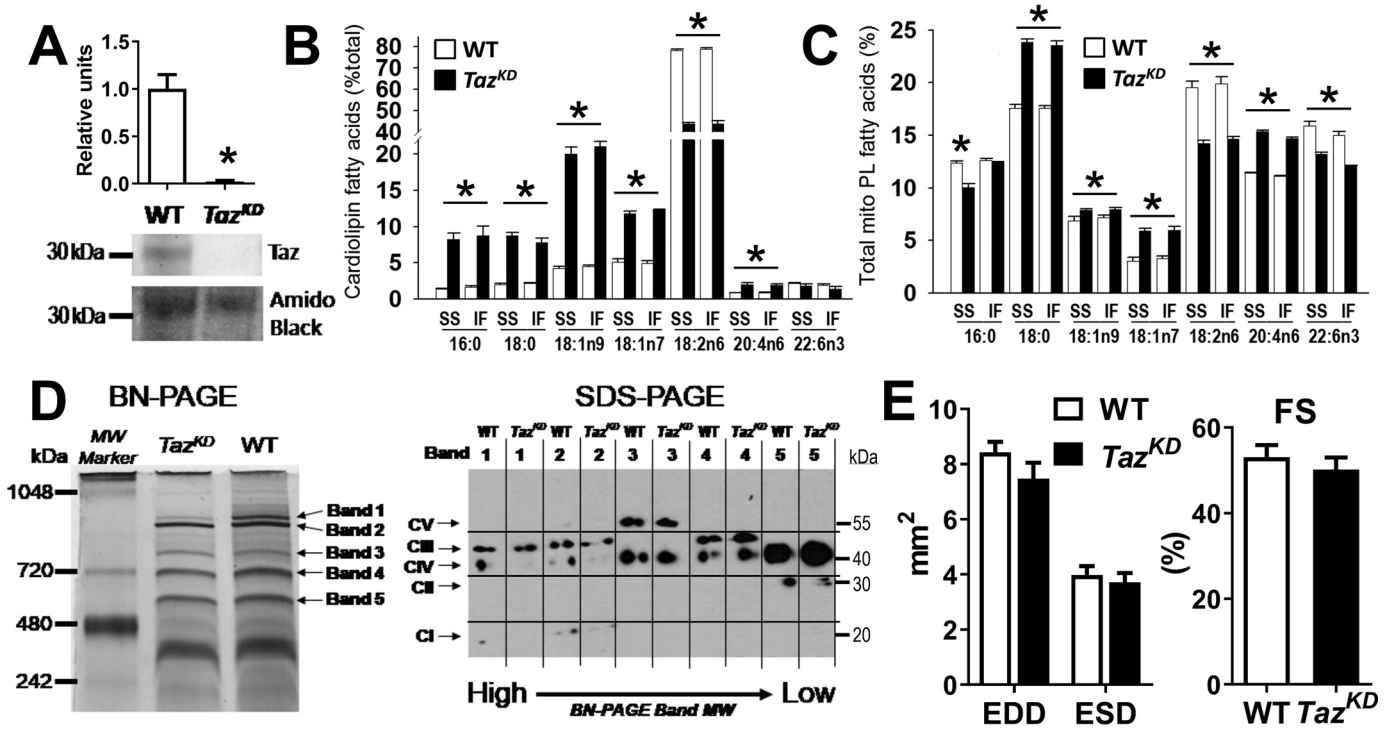

Figure 1. *Taz* deficiency disrupts mitochondrial membrane composition and supercomplex integrity but not cardiac function. *A*, graphical summary ($n = 6$/group) and representative immunoblot of ~30-kDa tafazzin protein detected in cardiac mitochondria from WT mice, but not *Taz* shRNA (*Taz*^{KD}) mice. *B* and *C*, fatty acid composition of cardiolipin (*B*) and total phospholipids (*PL*, *C*) extracted from SS and IF cardiac mitochondria ($n = 4$–6/group). *D*, representative images of high-molecular-mass protein complexes separated from WT and *Taz*^{KD} cardiac mitochondria by blue native (*BN*)–PAGE, subsequently probed for respiratory chain complexes I–V by SDS-PAGE (full analysis in Fig. S2). *E*, echocardiographic measures of left ventricular end-diastolic dimensions (*EDD*) and end-systolic dimensions (*ESD*) and corresponding fractional shortening (*FS*; [(EDD − ESD)/EDD × 100]) for 4–6-month-old WT and *Taz*^{KD} mice ($n = 12$/group). *, $P <$ 0.01 for WT *versus* *Taz*^{KD}.

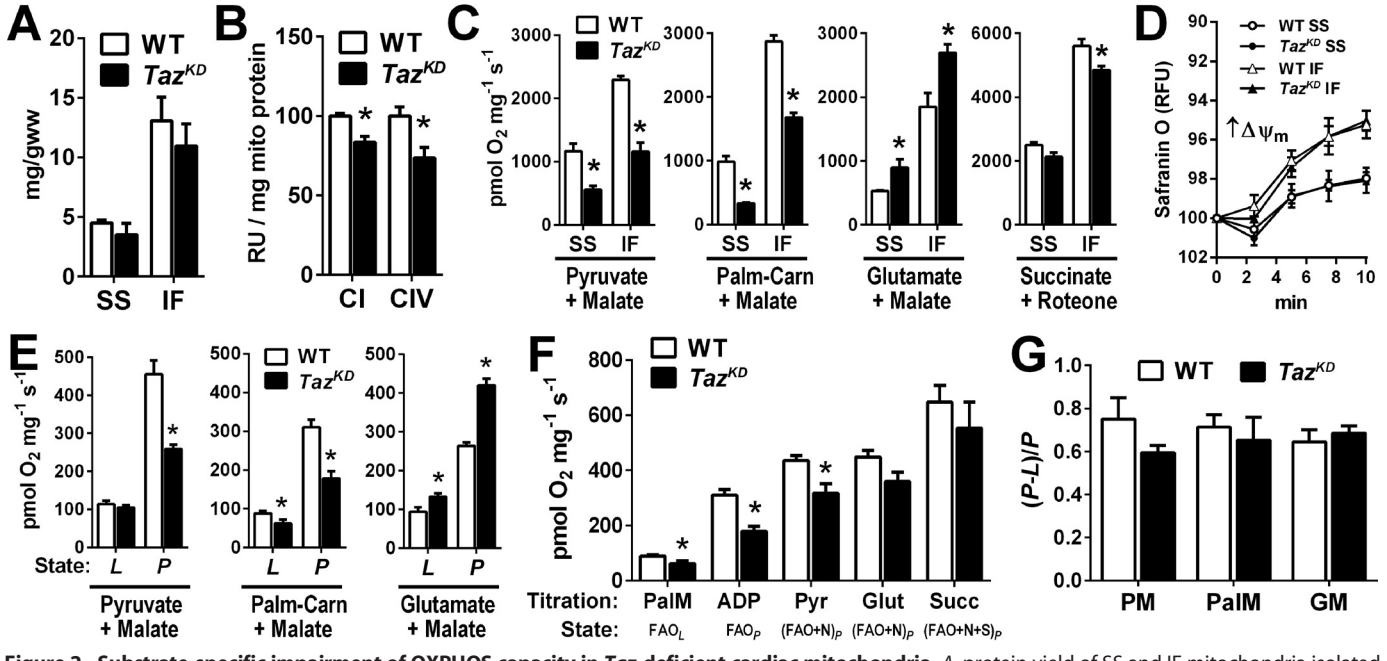

Figure 2. Substrate-specific impairment of OXPHOS capacity in *Taz*-deficient cardiac mitochondria. *A*, protein yield of SS and IF mitochondria isolated from WT and *Taz*^{KD} mouse hearts. *B*, spectrophotometric assessment of cytochrome *c* oxidase enzymatic activity from SS and IF mitochondria. *C*, state III respiration of isolated SS and IF cardiac mitochondria stimulated by 250 μM ADP, supported by the indicated substrates. *D*, membrane potential ($\Delta\Psi$) of isolated SS and IF mitochondria energized with succinate + rotenone determined by safranin O fluorescence quenching. *E*, maximal rates of LEAK (*L*, no ADP) and OXPHOS-linked respiration (*P*, 4 mM ADP-stimulated) in permeabilized cardiac muscle fibers supported by the indicated substrates. *F*, high-resolution respirometry substrate titration protocol generating multiple respiratory states in permeabilized cardiac fibers (see text for details). *G*, ADP respiratory control factors [$(P - L)/P$] for pyruvate + malate (*PM*), palmitoylcarnitine + malate (*PalM*), and glutamate + malate (*GM*) in WT and *Taz*^{KD} cardiac muscle fibers. The data are means ± S.E. ($n = 6$–8/group). *, $P < 0.05$ *Taz*^{KD} *versus* WT. *Carn*, carnitine; *Glut*, glutamate; *Palm*, palmitoylcarnitine; *Pyr*, pyruvate; *Succ*, succinate.

complex I (NADH dehydrogenase; CI) and complex IV (cytochrome *c* oxidase; CIV) were 16 and 26% lower in Taz^{KD} *versus* WT mitochondria, respectively (Fig. 2*B*), whereas state III (ADP-stimulated) respiration rates supported by CI-dependent pyruvate and palmitoylcarnitine (+ malate) were 41–66% lower in Taz^{KD} *versus* WT (Fig. 2*C*). However, state III respiration supported by glutamate + malate, which is also CI-dependent, was 45–68% *higher* in Taz^{KD} compared with WT mitochondria, reaching rates similar to those achieved with pyruvate and palmitoylcarnitine in WT. State III respiration with succinate + rotenone (supplying electrons though succinate dehydrogenase; CII) far exceeded rates with other substrates and was slightly lower in Taz^{KD} *versus* WT mitochondria, whereas mitochondrial membrane potential was identical between cohorts (Fig. 2*D*).

To confirm that the results obtained from mitochondria were not artifacts of the isolation procedure, high-resolution respirometry experiments were performed on permeabilized cardiac fibers with intact mitochondrial matrices. Indeed, similar substrate-specific defects in maximal (5 mM) ADP-stimulated respiration (P) were observed with pyruvate and palmitoylcarnitine (+ malate), whereas rates supported by glutamate + malate were higher in Taz^{KD} *versus* WT cardiac fibers (Fig. 2*E*). Cumulative titration of malate, palmitoylcarnitine, ADP, and pyruvate supported a lower integrated-substrate oxidative phosphorylation (OXPHOS)–linked respiration rate in Taz^{KD} *versus* WT fibers, which was largely restored by the addition of glutamate and succinate (Fig. 2*F*). OXPHOS coupling control factors derived from respiratory rates in the absence (*L*) and presence (*P*) of ADP ($1 - L/P$) were similar between Taz^{KD} and WT across multiple substrates, indicating no effect of tafazzin deficiency on OXPHOS coupling control (Fig. 2*G*). Collectively, these studies demonstrate that despite inducing a loss of L_4CL, CI–CIII–CIV supercomplexes and respiratory enzyme capacities, tafazzin deficiency does not intrinsically impair cardiac mitochondrial respiratory capacity but rather selectively impairs the oxidation of fatty acids and pyruvate and induces a compensatory increase in glutamate oxidation capacity.

Tafazzin deficiency increases mitochondrial oxidant production and damage

Several lines of evidence have linked impaired cardiolipin remodeling and supercomplex instability with increased production of mitochondrial reactive oxygen species (mtROS). Therefore, we evaluated mtROS release during OXPHOS-linked respiration by monitoring H_2O_2 emission from cardiac mitochondria (SS + IF populations) using the Amplex Red fluorometric assay coupled to our Oroboros oxygraph chamber (Fig. 3, *A* and *B*). mtROS release was higher in Taz^{KD} *versus* WT during maximal OXPHOS-linked respiration supported by CI + CII substrates (malate, pyruvate, glutamate, and succinate; *N* + *S*), and elevated further by inhibition of CI with rotenone (*S*). Similar results were seen in the presence of palmitoylcarnitine, implicating downstream sites in the respiratory chain as the primary source of greater ROS release from Taz^{KD} *versus* WT mitochondria during OXPHOS supported by mixed substrates. Consistent with these findings, high-molecular-mass (≥90 kDa) 4-hydroxynonenal-protein adducts and protein carbonyls were greater in Taz^{KD} *versus* WT mitochondria isolated from freshly harvested hearts (Fig. 3, *C* and *D*), indicating chronic elevation of mitochondrial oxidative stress *in vivo*. The absence of evidence for oxidative damage in lower-molecular-mass mitochondrial proteins might indicate their tendency to destabilize or be degraded by Lon protease as discussed below.

Tafazzin deficiency disrupts cardiac mitochondrial CoA metabolism

Pyruvate and palmitoylcarnitine both require CoA to support OXPHOS in mitochondria, whereas glutamate + malate can be oxidized to generate NADH by CoA-independent reactions via the malate–aspartate shuttle (31). Therefore, we hypothesized that tafazzin deficiency may alter mitochondrial CoA metabolism or availability. Indeed, we found that levels of free CoA in cardiac mitochondria (Fig. 4*A*) and tissue (Fig. 4*B*) were 40–50% lower in Taz^{KD} than WT. Similarly, tissue levels of pantothenic acid, the essential B-vitamin precursor of CoA, were also 40% lower in Taz^{KD} compared with WT hearts (Fig. 4*C*). Total acyl-CoA content (pmol/mg protein) assessed by LC–MS was also lower in snap-frozen Taz^{KD} hearts (Fig. 4*D*), which mainly reflected lower levels of long-chain acyl-CoAs (C13–20) and acetyl-CoA (Fig. 4*E*). Relative to total tissue acyl-CoA content, the proportions of short- and medium-chain acyl-CoAs were greater in Taz^{KD} *versus* WT, whereas long-chain species tended to decline Fig. 4*F*. However, a 93% higher relative proportion of 3-hydroxy-16:0-CoA was seen in Taz^{KD} *versus* WT (Fig. 4*G*), suggesting a site-specific defect in long-chain fatty acid oxidation. A full listing of individual acyl-CoAs detected by LC–MS in Taz^{KD} and WT hearts is presented in Table S1.

Mitochondrial proteomics reveals distinct pattern of metabolic remodeling in tafazzin deficiency

To explore the basis for the observed effects of tafazzin deficiency on mitochondrial metabolism, we performed targeted LC–MS/MS proteomic profiling of WT and Taz^{KD} mitochondria isolated from freshly harvested hearts. A total of 158 mitochondrial proteins met strict criteria for confident identification against the mouse Uniprot protein database (FDR, 0.1%), 103 of which were sorted based on functional annotations linking them to respiratory complexes or major energy metabolism pathways (Table S2). The majority of these are presented in Fig. 5*A* for interpretive analysis. Comparison of combined spectral counts from subunits representing individual respiratory chain complexes revealed a significant (22%) loss of total CI protein in Taz^{KD} *versus* WT per mg of total protein ($p < 0.05$), but no significant differences in complexes II, III, and IV or ATP synthase (Fig. 5*B*). Among the 33 CI subunits detected, those localized to the proximal membrane domain or "heel" of the complex were collectively lower by ~20–40% in Taz^{KD} *versus* WT mitochondria (Fig. 5*C*). Subunits in the distal membrane domain and peripheral arm were relatively unaffected, with the exception of NDUFA12 (B17.2) and NDUFA9 (39 kDa), which link catalytic subunits in the arm to core subunits in the membrane domain (32, 33). This selective loss of CI subunits

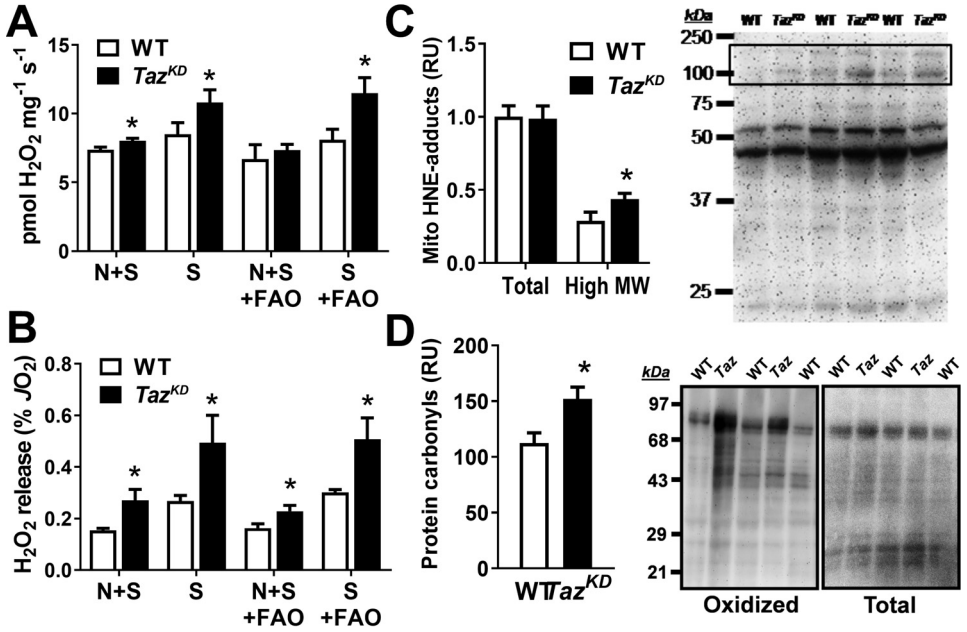

Figure 3. ***Taz*** **deficiency increases cardiac mitochondrial oxidant production and damage.** *A* and *B*, H_2O_2 release from cardiac mitochondria expressed per mg mito protein (*A*) or as a percentage of total oxygen consumption rate (*B*) during OXPHOS supported by complex I + II substrates (malate, pyruvate, glutamate, succinate, and ADP; *N* + *S*) or complex II alone (N + S + rotentone; *S*) in the presence or absence of fatty acid (palmitoylcarnitine) (*FAO*). *C*, total mitochondrial 4-hydroxynonenal–protein adducts were similar between genotypes, but high-molecular-mass (*High MW*) bands (*boxed region*) were greater in Taz^{KD} *versus* WT. *D*, mitochondrial protein carbonyls (oxidized proteins) were elevated in Taz^{KD} *versus* WT for similar quantity of total protein. The data are means ± S.E. (n = 4–8/group). *, $P < 0.05$ Taz^{KD} *versus* WT.

suggests destabilization of the complex, consistent with its depletion from CI–CIII–CIV supercomplexes (Fig. 1*D*). This might result in part from oxidation of CI proteins by mtROS (Fig. 3) and subsequent degradation by Lon protease (34), which was 3.5-fold higher in Taz^{KD} *versus* WT mitochondria (Fig. 5*D*).

Several enzymes involved in fatty acid oxidation were differentially affected by tafazzin deficiency, reflecting a specific reorganization of acyl-CoA metabolism (Fig. 5*E*). In particular, Taz^{KD} mitochondria exhibited >50% lower levels of long-chain acyl-CoA synthetase and moderately (11%) lower levels of very-long-chain acyl-CoA dehydrogenase ($p \leq 0.05$), consistent with impaired oxidation of long-chain fatty acids. Medium-chain acyl-CoA dehydrogenase (MCAD) and the dienoyl-CoA reductase were also 25–30% lower in Taz^{KD}, consistent with an accumulation of short- and medium-chain acyl-CoAs and specifically 10:1-CoA (Table S1). However, acyl-CoA thioesterases 2 and 13, both selective for long-chain acyl-CoAs (35, 36), were significantly (90%) higher in Taz^{KD} mitochondria (Fig. 5*F*), along with 20% greater levels of trifunctional protein-β (TFP-β) (Fig. 5*E*). TFP-β catalyzes the CoA-thiolysis of long-chain keto acyl-CoAs generated by the α-subunit, representing the final reaction of the inner membrane long-chain fatty acid β-oxidation cycle (37). Interestingly, TFP-α also possesses monolysocardiolipin acyltransferase activity (38), and the observed accumulation of 3-hydroxy-16:0-CoA in Taz^{KD} hearts suggests a specific block in the α-subunit's β-oxidation function (37).

Despite markedly lower pyruvate oxidation capacity of Taz^{KD} *versus* WT mitochondria (Fig. 2), the combined spectral count of the pyruvate dehydrogenase complex proteins was greater in Taz^{KD}, largely because of 43% higher levels of the E2 subunit responsible for acetyl-CoA formation (Fig. 5*G*). Tricarboxylic acid cycle enzymes were not uniformly affected by tafazzin deficiency but collectively tended to increase because of the 40% higher levels of malate dehydrogenase (MDH) (Fig. 5*H*). Notably, MDH is responsible for NADH production from glutamate oxidation in the malate–aspartate shuttle (MAS) (31, 39), which was also ~40% higher in Taz^{KD} compared with WT mitochondria (Fig. 2). To determine whether tafazzin deficiency increases cardiac availability of amino acids as anaplerotic substrates, we performed targeted GC/MS metabolite analysis of snap-frozen cardiac samples from Taz^{KD} and WT mice. Indeed, all amino acids were higher in Taz^{KD} except for proline (lower) and glutamate (unchanged) (Fig. 5*I*), consistent with a greater utilization of glutamate to maintain anaplerotic flux in the face of impaired pyruvate and fatty acid oxidation. Taken together, these analyses corroborate our functional evidence for a selective defect in CoA metabolism and a rearrangement of substrate oxidation pathways favoring glutamate utilization in tafazzin-deficient cardiac mitochondria.

Exogenous CoA supplementation partially rescues fatty acid and pyruvate oxidation in Taz^{KD} mitochondria

To further investigate how tafazzin deficiency impairs fatty acid oxidation capacity, we evaluated OXPHOS rates of Taz^{KD} and WT mitochondria supported by substrates entering the pathway at specific sites (Fig. 6*A*). Palmitoylcarnitine bypasses carnitine palmitoyltransferase 1 (CPT1) for β-oxidation initially by the long-chain-specific system on the inner mitochondrial membrane (very-long-chain acyl-CoA dehydrogenase and TFP), followed by the medium- and short-chain acyl-CoA dehydrogenases in the canonical matrix β-oxidation cycle (Fig.

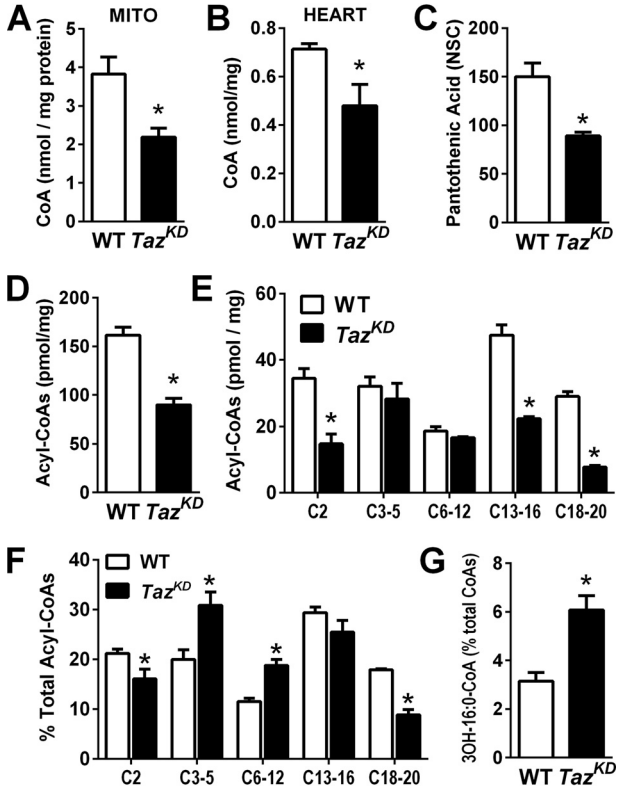

Figure 4. *Taz* deficiency disrupts cardiac acyl-CoA metabolism. *A* and *B*, free CoA content of isolated cardiac mitochondria (*MITO*, *A*) and snap-frozen cardiac tissue (*B*) from WT and Taz^{KD} mice. *C* and *D*, pantothenic acid levels (*C*) and total acyl-CoAs (*D*) in cardiac tissue. *E* and *F*, acyl-CoAs grouped by number of carbons ranging from acetyl-CoA (C2) to 18–20 carbon acyl-CoAs (C18–20) expressed per mg tissue (*E*) and as a percentage of total acyl-CoAs (*F*). *G*, 3-OH-palmitoyl-CoA accumulates relative to total acyl-CoA content in Taz^{KD} *versus* WT. The data are means ± S.E. (n = 4–6/group). *, $P < 0.05$ Taz^{KD} *versus* WT.

5*A*). Similar to results from SS and IF mitochondria and permeabilized fibers (Fig. 2), maximal palmitoylcarnitine-supported OXPHOS in a combined (SS + IF) mitochondrial fraction from Taz^{KD} hearts was ~58% of WT ($p < 0.01$; Fig. 6, *A* and *B*). Oxidation of C8 octanoylcarnitine, which bypasses CPT1 and the long-chain β-oxidation system for oxidation by MCAD, was similarly lower in Taz^{KD}, arguing against an isolated rate-limiting defect in long-chain fatty acid oxidation. Surprisingly, oxidation of palmitoyl-CoA + carnitine, which requires CPT1 activity, was not significantly lower in Taz^{KD} than WT, arguing against a rate-limiting defect in mitochondrial fatty acid transfer.

Given evidence for lower CoA levels in Taz^{KD} mitochondria, we hypothesized that exogenous supply of CoA might have contributed to the higher relative (Taz^{KD}/WT) oxidation rates with palmitoyl-CoA compared with acylcarnitines (Fig. 6*B*), because free CoA is readily transported into isolated cardiac mitochondria (40). Indeed, preincubation of mitochondria with CoA using an established protocol (40) increased levels ~2-fold in Taz^{KD} and WT mitochondria, restoring CoA in Taz^{KD} to untreated WT levels (Fig. 6*C*). This CoA enrichment increased OXPHOS-linked respiratory capacity supported by pyruvate + malate (*ADP* in Fig. 6*D*), palmitoylcarnitine + malate (*ADP* in Fig. 6*E*), and their combination (*Pyr* in Fig. 6*E*) in Taz^{KD} mitochondria. There were no effects of CoA enrichment on WT mitochondrial function, suggesting that physiological CoA levels are sufficient to support maximal OXPHOS. Collectively, these studies implicate mitochondrial CoA availability as a primary limitation of maximal carbohydrate and fatty acid oxidation capacity in tafazzin-deficient cardiac mitochondria.

Discussion

This study sought to elucidate how impaired cardiolipin remodeling impacts cardiac mitochondrial function and identify potentially compensatory adjustments to tafazzin deficiency that manifest prior to development of cardiac dysfunction. The *Taz* shRNA mouse proved ideal for this purpose, exhibiting persistent depletion of L_4CL and CI–CIII–CIV mitochondrial supercomplexes characteristic of BTHS (14, 41) and other cardiac pathologies (42, 43) but preserved cardiac function well into adulthood. The results confirmed moderate impairment of CI and CIV enzymatic capacities in Taz^{KD} mitochondria that parallel findings from BTHS patient–derived cell lines and are consistent with a loss of CI subunits (Fig. 5) and previous links between L_4CL content and CIV activity (44, 45). However, isolated respiratory enzyme capacities far exceed the activity required to support maximal OXPHOS rates, such that moderate reductions might not impair intact mitochondrial energetics (46). Indeed, although maximal CI-dependent OXPHOS supported by pyruvate or palmitoylcarnitine (+ malate) was lower in Taz^{KD}, CI-dependent glutamate + malate OXPHOS approximated rates obtained in WT with other CI substrates, implicating defects upstream of the respiratory chain. Similarly, succinate-supported OXPHOS was slightly lower in Taz^{KD}, consistent with a CII defect in this model (21), but multisubstrate CI+II-linked OXPHOS in permeabilized heart fibers was not significantly impaired. Therefore, although tafazzin deficiency clearly impairs respiratory enzyme capacity, these defects are evidently insufficient to limit integrated OXPHOS-linked respiratory capacity in intact mitochondria. These findings are consistent with normal basal rates of mitochondrial respiration, ATP synthesis, and tricarboxylic acid cycle flux recently reported from BTHS patient–derived cell lines (30) and suggest that mechanisms other than overt bioenergetic failure contribute to the pathogenesis of BTHS.

The CL-dependent assembly of respiratory supercomplexes has been postulated to improve electron channeling between individual complexes, such that disruption might impair OXPHOS efficiency or increase mtROS formation (47). We found no difference in the capacity of Taz^{KD} *versus* WT mitochondria to maintain high membrane potential in the absence of ADP (Fig. 2*D*), nor the degree of OXPHOS coupling control by ADP with any substrates (Fig. 2*G*), suggesting that tafazzin/cardiolipin deficiency and CI/III/IV supercomplex instability do not impair the efficiency of OXPHOS or proton pumping. However, mtROS release during OXPHOS was significantly greater from Taz^{KD} *versus* WT mitochondria and paralleled greater accumulation of mitochondrial protein carbonyls and 4-hydroxynonenal–protein adducts. Neither the addition of fatty acid or inhibition of CI by rotenone altered the magnitude

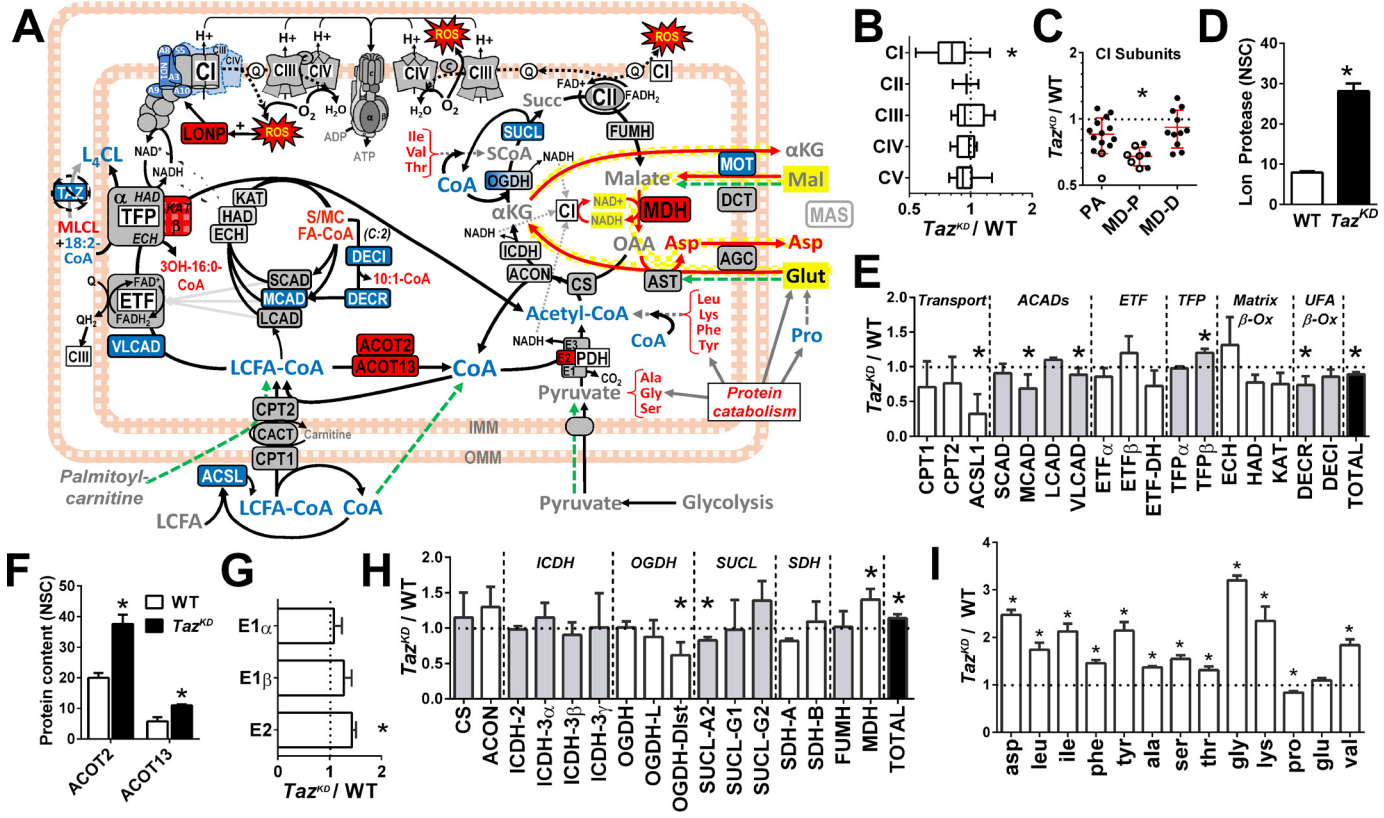

Figure 5. Remodeling of the mitochondrial proteome in the *Taz*-deficient heart. *A*, summary schematic illustrating enzymes (*boxes*) found by LC–MS proteomic profiling of cardiac mitochondria to be higher (*red fill*), lower (*blue fill*), or not different (*gray fill*) in Taz^{KD} compared with WT mice ($q < 0.05$; $n = 3$/group). Metabolites detected by GC/MS in snap-frozen cardiac tissue are shown in *red* ($Taz^{KD} >$ WT), *blue* ($Taz^{KD} <$ WT), *black* ($Taz^{KD} =$ WT), or *gray font* (not measured, but included for context) ($q < 0.05$; $n = 4$–6/group). *Green dashed arrows* indicate entrance sites of exogenous substrates added in mitochondrial respiration experiments, with glutamate oxidation through the MAS highlighted in *yellow*. *B–I*, graphical data representing the relative (Taz^{KD}/WT) expression of cumulative normalized spectral counts corresponding to: respiratory chain complexes (*B*); complex 1 subunits localized to the peripheral arm (*PA*), proximal (*MD-P*), and distal membrane domain (*MD-D*) (*C*); Lon protease (*LONP*) (*D*); fatty acid oxidation enzymes (*E*); acyl-CoA thioesterases (*ACOT*) 2 and 13 (*F*); pyruvate dehydrogenase (*PDH*) complex subunits (*G*); tricarboxylic acid cycle enzymes (*H*); and cardiac free amino acid content (per mg tissue protein) detected by GC/MS (*I*). *, $q < 0.05$ Taz^{KD} *versus* WT. *ACADs*, acyl-CoA dehydrogenases; *ACON*, aconitase; *ACSL*, acyl-CoA synthetase; *AGC*, aspartate-glutamate cotransporter; *AST*, aspartate transaminase; *CACT*, carnitine-acyl-CoA translocase; *CS*, citrate synthase; *DCT*, dicarboxylate transporter; *DECR*, dienoyl-CoA reductase; *DECI*, dienoyl-CoA isomerase; *ECH*, enoyl-CoA hydratase; *ETF*, electron transferring flavoprotein; *FUMH*, fumarate hydratase; *HAD*, hydroxyacyl-CoA dehydrogenase; *ICDH*, isocitrate dehydrogenase; *KAT*, ketoacyl-CoA thiolase; *OGDH*, oxoglutarate dehydrogenase; *LCFA*, long-chain fatty acid; *MOT*, malate-oxogluarate transporter; *SUCL*, succinyl-CoA ligase.

of this effect, suggesting that site(s) downstream of CI in the respiratory chain are the primary source of greater mtROS release from Taz^{KD} mitochondria. We postulate that impaired linkage of CI to CIII–CIV supercomplexes drives greater mtROS generation and an accumulation of oxidative damage that ultimately impairs cardiac function in Taz^{KD} mice by 8–10 months of age (24, 25), consistent with the mechanistic role of excess ROS in cardiomyocyte dysfunction demonstrated by *in vitro* models of tafazzin deficiency (18, 48).

The healthy mammalian heart relies almost exclusively on the oxidation of long-chain fatty acids and pyruvate to meet its energy demands (49). However, cardiomyocytes also readily oxidize glutamate via the MAS, which plays a key role in coordinating cytosolic and mitochondrial redox balance and energy homeostasis (50), particularly under states of metabolic stress (*e.g.* ischemia reperfusion) (31). MAS activity is governed largely by the availability of glutamate and α-ketoglutarate dehydrogenase (OGDH) activity, whereby reduced flux through OGDH directs α-ketoglutarate to the MAS, facilitating uptake and oxidation of malate by MDH (50). The up-regulation of glutamate oxidation capacity in Taz^{KD} mitochondria herein was associated with lower expression of the Dlst (CoA-binding) subunit of the OGDH complex and higher MDH expression, consistent with a compensatory shift in tricarboxylic acid flux to favor higher MAS activity. This finding is corroborated by a specific destabilization of the OGDH complex in human BTHS cells, without impairment of cellular respiration or ATP production (30). We postulate that these changes reflect an adaptive reorganization of oxidative pathways to compensate for deficient pyruvate and fatty acid oxidation in tafazzin-deficient mitochondria, perhaps partially offsetting the bioenergetic stress of suboptimal cardiac fuel utilization. Indeed, greater capacity for systemic proteolysis and amino acid oxidation is associated with reduced cardiac systolic strain in BTHS patients (51). It is also noteworthy that the brain exhibits constitutively high MAS activity and glutamate oxidation capacity (52) and is relatively unaffected in BTHS despite being a primary locus of pathology in other mitochondrial disorders (53).

Elucidating how tafazzin deficiency impairs oxidation of fatty acids and pyruvate, but not glutamate, is of considerable

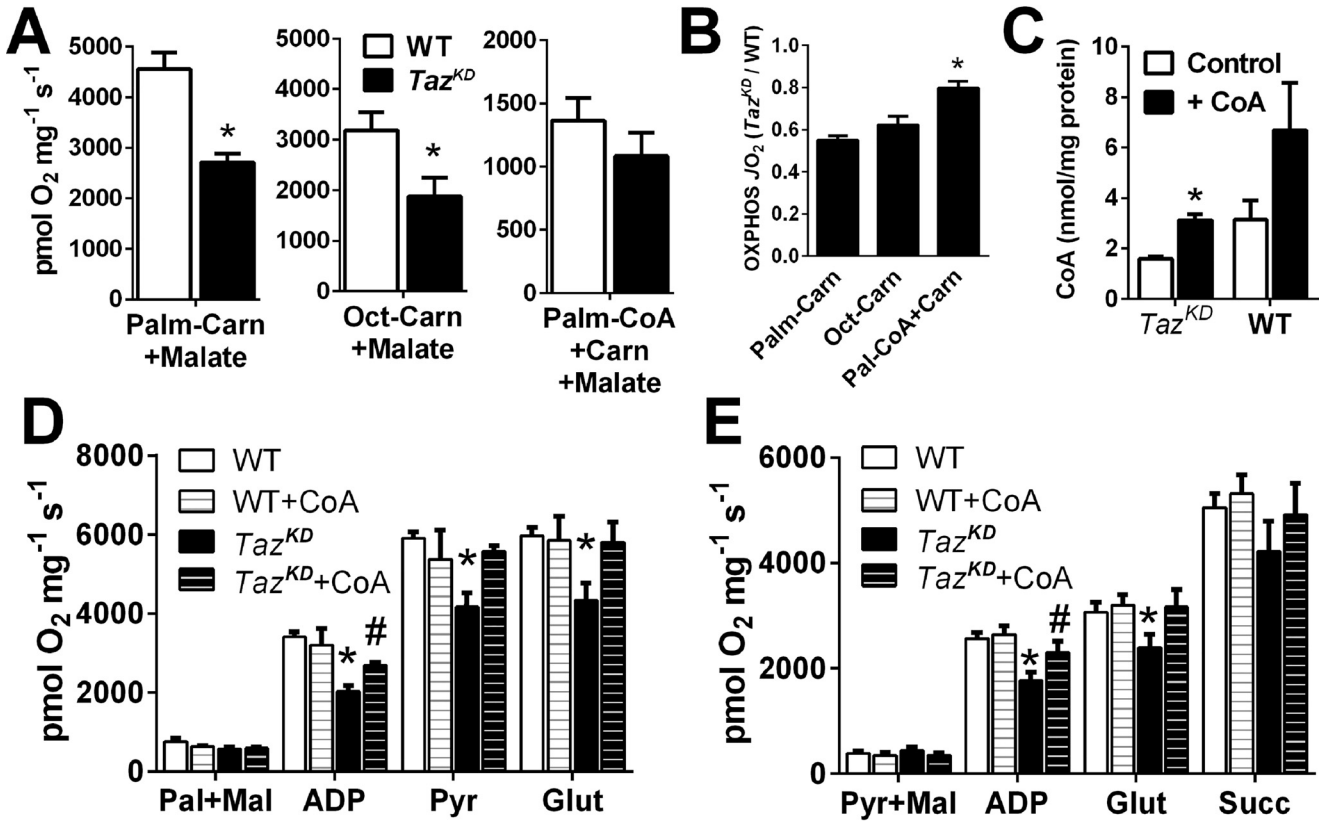

Figure 6. Exogenous CoA partially rescues respiratory function of tafazzin-deficient cardiac mitochondria. *A* and *B*, OXPHOS-linked respiratory capacity of cardiac mitochondria supported by CPT1-independent long-chain (palmitoyl; *Palm*) or medium-chain (octanoyl; *Oct*) acylcarnitines, or CPT1-dependent palmitoyl-CoA + carnitine expressed as O_2 flux/mg protein (*A*), and relative activity between genotypes (Taz^{KD}/WT; *B*) (n = 4–5/group). *C–E*, exogenous CoA incubation (+ CoA) increases mitochondrial CoA content in Taz^{KD} mitochondria (*C*) and partially restores OXPHOS capacity of Taz^{KD} mitochondria fueled by palmitoylcarnitine + malate (ADP in *D*) or pyruvate + malate (ADP in *E*) in cumulative substrate titration respirometry protocols. The data are means ± S.E. (n = 4–6/group). *, $P < 0.05$ Taz^{KD} *versus* all groups. #, $P < 0.05$ Taz^{KD} *versus* Taz^{KD} + CoA. *Carn*, carnitine; *Glut*, glutamate; *Pyr*, pyruvate; *Succ*, succinate.

scientific and clinical interest, because this remains a severe limitation to optimal cardiac bioenergetics in BTHS (54). Results from the present study suggest a potential block in medium-chain acyl-CoA oxidation in Taz^{KD} mitochondria, given evidence for similar impairment of both long- and medium-chain acylcarnitine oxidation, lower MCAD expression, and a relative accumulation of C3-C12 acyl-CoAs. Protein levels of the pyruvate dehydrogenase complex subunits were not lower in Taz^{KD}, but this enzyme complex has been previously shown to be inhibited by post-translational modifications in this and other *Taz*-deficient models (55). However, partial rescue of both palmitoylcarnitine- and pyruvate-supported OXPHOS flux with exogenous CoA herein suggests additional limitations imposed by free CoA availability or impaired CoA-dependent reactions. Up-regulation of long-chain–specific ACOT 2 and 13 could reflect mitochondrial CoA "trapping" by incompletely oxidized acyl-CoAs, perhaps resulting from a block in long-chain fatty acid oxidation by TFP indicated by accumulation of 3OH-16:0-CoA and up-regulation of its β-subunit (37). TFP requires free CoA for activity and also catalyzes transfer of acyl-CoA to monolysocardiolipin (38, 56), which accumulates in Taz^{KD} mitochondria, potentially interfering with its β-oxidation function. Whether the global decrease in mitochondrial CoA-esters reflects an impairment or compensatory down-regulation of CoA metabolism is unclear, but several aspects of the BTHS phenotype align with systemic CoA/pantothenate deficiency (57). Within this context, the therapeutic value of pantothenate supplementation has been explored in BTHS patients with mixed success, perhaps reflecting defects in the uptake or utilization of B vitamins (57, 58). Our CoA rescue experiments demonstrate *Taz*-deficient mitochondria retain the ability to import CoA, at least *in vitro*, further implicating an upstream decrease in CoA biosynthesis and/or pantothenate availability that merits future investigation. Although the mechanism of CoA deficiency remains unclear, we postulate that defects in mitochondrial handling of acyl-CoAs play a central role in the metabolic defects induced by tafazzin deficiency. The successful up-regulation of CoA-independent glutamate oxidation in Taz^{KD} mice strongly supports this hypothesis, despite evidently being insufficient to meet bioenergetic demands in BTHS patients (54).

In summary, our studies reveal that defective cardiolipin metabolism resulting from tafazzin deficiency selectively impairs pyruvate and fatty acid oxidation but elicits compensatory up-regulation of glutamate oxidation by the MAS that is capable of supporting normal rates of OXPHOS-linked respiration in cardiac mitochondria. This occurs despite expected reductions in respiratory enzyme capacities and supercomplex instability, implicating upstream defects in specific substrate oxidation pathways as the primary limitation of normal bioenergetics in

tafazzin-deficient hearts. Depletion or "trapping" of mitochondrial CoA secondary to disruptions of acyl-CoA metabolism likely contribute to this phenotype, with potential implications for the future investigation and treatment of BTHS. However, early and persistent elevations in mtROS release and oxidative stress may ultimately supersede bioenergetic defects in the pathogenesis of cardiomyopathy, consistent with previous reports from other BTHS models. Taken together, these studies provide new insights and perspective on how tafazzin and cardiolipin metabolism influence mitochondrial function in the mammalian heart, which should be considered along with advances contributed by lower-order and *in vitro* model systems.

Experimental procedures

Animal model

Doxycycline-inducible *Taz* shRNA (Taz^{KD}) mice, originally generated at TaconicArtemis, GmbH (Köln, Germany) under contract from the Barth Syndrome Foundation, were obtained from Dr. Zaza Khuchua at the University of Cincinnati (24) and used to establish a colony of Taz^{KD} and WT mice at Colorado State University for these studies. Both Taz^{KD} and WT mice were maintained on RMH1500 chow (Purina, Gray Summit, MO) supplemented with 625 mg/kg doxycycline to induce *Taz* shRNA expression and control for any unintended effects of doxycycline in WT mice. Transgenic males were mated with WT females, and the offspring were genotyped by PCR analysis of tail DNA using previously described sequences (24). The extent of tafazzin knockdown in cardiac mitochondria was initially performed by quantitative RT-PCR and confirmed by immunoblotting for tafazzin protein using a mAb (Santa Cruz Biotechnology catalog no. sc-365810). *Taz* shRNA positive mice were studied along with WT littermates at 4–5 months of age, when the mice exhibited significant cardiolipin and mitochondrial abnormalities but no overt cardiac dysfunction (24, 25). Only male mice were used to model the X-linked inheritance of BTHS in humans. The mice were deeply anesthetized with 100 mg/kg sodium pentobarbital intraperitoneally prior to sacrifice by midline thoracotomy and removal of the heart. All procedures were approved by the Colorado State University Care and Use Committee and conform to the Guide for the Care and Use of Laboratory Animals published by the U.S. National Institutes of Health (publication 85-23, revised 1996).

Echocardiography

Transthoracic echocardiography was performed under light (1.5%) isoflurane anesthesia using a 15-MHz linear array transducer connected to a Phillips HD11 ultrasound. Short-axis 2D images of left ventricular end-diastolic and end-systolic areas were obtained for assessment of left ventricular chamber morphology and fractional shortening ((end-diastolic area − end-systolic area)/end-diastolic area) × 100). The data were averaged from four consecutive high-resolution cycles by the same technician.

Mitochondrial preparations

Mitochondria were freshly isolated from ~75–90 mg of heart tissue by differential centrifugation methods previously described (59). For some experiments, SS and IF mitochondria were isolated using trypsin to dissociate IF mitochondria from myofibrillar proteins (59). To evaluate the respiratory function of intact cardiac mitochondrial matrices *in situ*, structurally sound fiber bundles (1.0 – 1.2 mg) were dissected from 10–15-mg left ventricular sections and permeabilized with saponin as previously described (60). Permeabilized fiber bundles were gently blotted dry on Whatman paper for 10–15 s to remove excess buffer, weighed, and immediately placed in the Oxygraph chamber. Respirometry data from permeabilized fibers are normalized to fiber weight, whereas data from isolated mitochondria are expressed per mg of mitochondrial protein determined by BCA assay.

Mitochondrial phospholipid analyses

The fatty acid composition of total mitochondrial phospholipids, cardiolipin, phosphatidylcholine, and phosphatidylethanolamine was performed in lipids extracted from SS and IF mitochondrial fractions as previously described (59). Briefly, phospholipid classes were separated by normal phase liquid chromatography using a hexane:isopropanol:potassium acetate mobile phase gradient optimized for separation of phosphatidylethanolamine, phosphatidylcholine, and cardiolipin by UV detection (206 nm). Fractions were collected based on elution time of known standards, evaporated under a nitrogen stream, and resuspended in hexane, followed by the addition of 14% BF_3-methanol and heating at 100 °C for 30 min to obtain methyl esters for gas chromatographic analysis of fatty acid composition. Cardiolipin molecular species were analyzed by electrospray ionization MS as previously described in detail (61).

Mitochondrial supercomplexes

High-molecular-mass mitochondrial enzyme complexes were separated in their native state by blue native–PAGE using 4–15% polyacrylamide gradient Tris–glycine gels (Bio-Rad, Criterion TGX) for 1 h at 70 volts with blue cathode buffer to image and quantitate density of supercomplex bands. High-molecular-mass bands (>500 kDa) were excised, treated with Laemmli buffer and 2-mercaptoethanol, and loaded on to 4–20% Tris-HCl gels for separation of individual respiratory chain complex subunits by SDS-PAGE. Electrophoresed proteins were transferred to polyvinylidene difluoride membranes and blotted for OXPHOS complex levels using an antibody mixture that recognizes subunits from each of the five respiratory complexes (Abcam catalog no. ab110413). The bands were photographed by a UVP ChemiDoc imager and analyzed by ImageJ (National Institutes of Health).

Mitochondrial respirometry

State 3 (ADP-dependent) respiration corresponding to OXPHOS was assessed in freshly isolated mitochondria (75 μg of protein) at 37 °C in response to 50 μM ADP at an initial

oxygen concentration of 150 μM on an O2k high-resolution respirometer (Oroboros Instruments, Innsbruck, Austria). Multiple experiments were carried out in MiR06 buffer (60) using saturating concentrations of the following substrate combinations: pyruvate (5 mM) + malate (1 mM), palmitoylcarnitine (0.04 mM) + malate (1 mM), succinate (20 mM) + rotenone (100 nM), or malate (1 mM) + glutamate (10 mM). Oxygen flux was monitored in real time by resolving changes in the negative time derivative of the chamber oxygen concentration signal following standardized instrumental and chemical background calibrations using Datlab software (Oroboros Instruments). Respirometry studies in permeabilized fibers were conducted in a hyperoxygenated environment (275–400 μM) to avoid limitations in oxygen diffusion (62, 63) under the identical buffer and substrate conditions described above. For fibers and some mitochondrial studies, substrates were added in series as indicated under "Results," and 5 mM ADP was used to obtain maximal OXPHOS capacities under cumulative substrate conditions.

Mitochondrial enzyme activities and membrane potential

Enzymatic activities of respiratory complexes I and IV were determined in frozen-thawed mitochondrial isolates by monitoring the oxidation of NADH or cytochrome *c*, respectively, by previously described spectrophotometric methods (61) using a Spectramax M2e spectrofluorometer (Molecular Devices) normalized to total protein by the BCA assay (Pierce). Relative comparisons of mitochondrial membrane potential was performed in isolated mitochondria (33 μg of protein) energized with 20 mM succinate (+ rotenone) in reaction buffer containing 250 mM sucrose, 10 mM Tris-MOPS, and 0.01 mM EGTA, pH 7.4, with KOH, by monitoring quenching of 8 μM safranin O fluorescence (excitation/emission, 525/575 nm) at 2.5-min intervals for 10 min.

Mitochondrial H_2O_2 release and oxidative stress

The net rate of mitochondrial H_2O_2 release was determined during respirometry experiments by monitoring the accumulation of chamber resorufin (excitation/emission, 571/585 nm), the stable fluorescent product of 1:1 oxidation of Amplex UltraRed (AmR, Molecular Probes; 5 μM) by H_2O_2 in the presence of horseradish peroxidase (1 units/ml) (64) in our Oroboros respirometer. Resorufin fluorescence was calibrated to chamber [H_2O_2] using freshly prepared H_2O_2 standards (0.1–1 μM) stabilized with 10 μM HCl as previously described (65) and corrected for chemical background reactions in MiR05 respiration buffer (MiR06 without catalase) in the presence of respiratory substrates: 1 mM malate, 5 mM pyruvate, 10 mM glutamate, and 20 mM succinate, with or without 2.5 mM ADP. All data were collected between 180 and 200 μM O_2 to avoid confounding effects of different chamber O_2 concentrations on mtROS production. To assess the extent of chronic oxidative stress to mitochondria, 30 μg of mitochondrial protein were immunoblotted for 4-hydroxynonenal–protein adducts (Calbiochem; catalog no. 393207; 1:2000 dilution) and protein carbonyls (Oxyblot; Millipore Sigma S7150) quantified by densitometry (ImageJ, National Institutes of Health) following chemiluminescent imaging of bands using a UVP ChemiDoc imager (Upland, CA, USA).

Cardiac tissue and mitochondrial CoA content and supplementation studies

Mitochondrial CoA content was determined in isolated mitochondria using a commercially available colorimetric assay kit (BioVision; catalog no. K367-100) and normalized to mitochondrial protein by BCA assay. Acyl-CoAs were quantified in cardiac tissue homogenates by LC–MS using the method of Palladino *et al.* (66) on an API 4000 electrospray ionization mass spectrometer and an Acuity UPLC HILIC column (Waters, Milford, MA). To evaluate whether mitochondrial CoA content limited respiratory capacities of isolated mitochondria, respiratory studies were performed in mitochondrial suspensions preincubated with CoA as previously described to induce uptake and accumulation of CoA into the matrix of isolated rat cardiac mitochondria (40). Briefly, mitochondrial suspensions (200 μg of protein) freshly isolated from the same mouse heart were incubated in 200 μl of KME suspension buffer (100 mM KCl, 50 mM MOPS, 0.5 mM EGTA, pH 7.4) containing 8 mM ATP with or without 100 μM CoA at 30 °C for 20 min under gentle shaking. Following incubation, mitochondrial suspensions were cooled on ice and pelleted at 3000 × *g* at 4°C, resuspended in 200 μl of KME, and repelleted. The resulting mitochondrial pellets were washed and resuspended in 50 μl of KME, assayed for total protein and CoA content, and immediately used in respiration experiments as described above.

Mitochondrial proteomic profiling

Targeted LC–MS/MS analyses of mitochondrial proteins was performed in 30 μg of protein extracted from cardiac IF mitochondria isolated from Taz^{KD} and WT mice (n = 3/group). Trypsin-digested samples were subjected to offline UPLC-UV fractionation and concentration for LC–MS/MS analysis on a Thermo Scientific LTQ linear ion trap mass spectrometer. MS/MS spectra were searched against the mouse Uniprot protein database concatenated with reverse sequences for determination of the peptide FDR (118,690 sequence entries; 0.1%) using both the MASCOT database search engine (version 2.3) and Sorcerer™-SEQUEST® (67). A detailed description of the proteomic profiling and data analysis methods is provided in the supporting information.

Cardiac amino acid and pantothenate analysis

Six Taz^{KD} and WT mice were deeply anesthetized with sodium pentobarbital prior to rapid midline thoracotomy and freeze clamping of the beating heart within 10–15 s using a hemostat precooled in liquid nitrogen. The resulting ~30 mg frozen heart wafer was homogenized in 1 ml of methanol/water (70:30) and processed for GC/MS analysis using a Trace GC Ultra gas chromatograph coupled to a Thermo DSQ II mass spectrometer (Thermo Scientific) as described in detail in the supporting information. Molecular features were formed into peak groups using AMDIS software, and the spectra were screened in the National Institute for Technology Standards (www.nist.gov) and Golm (http://gmd.mpimp-golm.mpg.de/)

metabolite databases for identifications, validated comparing retention indices and mass spectra from heart extracts to databases of authentic standards (68, 69).

Statistical analyses

All data are presented as group means ± S.E. Group differences between Taz^{KD} and WT were examined by independent sample *t* tests with Bonferroni–Hochberg corrections for multiple comparisons (FDR, 0.05) for metabolite and proteomic profiling to denote statistical significance at $q < 0.05$ and a standard $p \leq 0.05$ for all other comparisons. Analyses of variance were used to determine significant differences between greater than two groups, followed by Tukey HSD post hoc test where appropriate for pairwise comparisons.

Data availability

Raw MS data are available online at 10.5281/zenodo.3932695.

Acknowledgments—We thank Carolyn Broccardo (Colorado State University) for assistance with the proteomic analyses, Cheyanne Izon and Philip Zilhaver (Colorado State University) for assistance with the immunoblotting, Victoria Harcy (Colorado State University) for assistance with maintenance of the TazKD mouse colony, and Michael J. Bennett (Children's Hospital of Philadelphia) for collaboration and technical assistance with optimizing the acyl-CoA analyses.

Author contributions—C. H. L., L. G. B., and A. J. C. conceptualization; C. H. L., S. M. C., K. C. C. , G. C. S., and A. J. C. resources; C. H. L., L. G. B., K. S. S., L. C. L. P., C. M. M., A. L. H., J. E. P., S. M. C., G. C. S., and A. J. C. data curation; C. H. L., L. G. B., K. S. S., C. M. M., A. L. H., J. E. P., S. M. C., G. C. S., and A. J. C. formal analysis; C. H. L., L. C. L. P., C. M. M., J. E. P., S. M. C., K. C. C., G. C. S., and A. J. C. supervision; C. H. L., L. G. B., and A. J. C. funding acquisition; C. H. L., L. G. B., K. S. S., L. C. L. P., C. M. M., A. L. H., J. E. P., K. C. C., G. C. S., and A. J. C. investigation; C. H. L., L. G. B., K. S. S., L. C. L. P., C. M. M., A. L. H., J. E. P., S. M. C., K. C. C., G. C. S., and A. J. C. methodology; C. H. L., L. G. B., and A. J. C. writing-original draft; C. H. L. and A. J. C. project administration; C. H. L., L. G. B., S. M. C., and K. C. C. writing-review and editing.

Funding and additional information—This work was supported by grants from the Barth Syndrome Foundation and a Scientist Development Grant from the American Heart Association (to A. J. C.).

Conflict of interest—The authors declare that they have no conflicts of interest with the contents of this article.

Abbreviations—The abbreviations used are: BTHS, Barth syndrome; CL, cardiolipin; L_4CL, tetra-linoleoyl cardiolipin; shRNA, short hairpin RNA; SS, subsarcolemmal; IF, intermyofibrillar; OXPHOS, oxidative phosphorylation; CI, complex I; CII, complex II; CIII, complex III; CIV, complex IV; mtROS, mitochondrial reactive oxygen species; FDR, false discovery rate; MCAD, medium-chain acyl-CoA dehydrogenase; TFP, trifunctional protein; MDH, malate dehydrogenase; MAS, malate–aspartate shuttle; CPT, carnitine palmitoyltransferase; OGDH, α-ketoglutarate dehydrogenase.

References

1. Bione, S., D'Adamo, P., Maestrini, E., Gedeon, A. K., Bolhuis, P. A., and Toniolo, D. (1996) A novel X-linked gene, G4.5. is responsible for Barth syndrome. *Nat. Genet.* **12,** 385–389 CrossRef Medline
2. Barth, P. G., Wanders, R. J., Vreken, P., Janssen, E. A., Lam, J., and Baas, F. (1999) X-linked cardioskeletal myopathy and neutropenia (Barth syndrome) (MIM 302060). *J. Inherit. Metab. Dis.* **22,** 555–567 CrossRef Medline
3. Hoch, F. L. (1992) Cardiolipins and biomembrane function. *Biochim. Biophys. Acta* **1113,** 71–133 CrossRef Medline
4. Fry, M., and Green, D. E. (1981) Cardiolipin requirement for electron transfer in complex I and III of the mitochondrial respiratory chain. *J. Biol. Chem.* **256,** 1874–1880 Medline
5. Robinson, N. C. (1993) Functional binding of cardiolipin to cytochrome *c* oxidase. *J. Bioenerg. Biomembr.* **25,** 153–163 CrossRef Medline
6. Zhang, M., Mileykovskaya, E., and Dowhan, W. (2002) Gluing the respiratory chain together. Cardiolipin is required for supercomplex formation in the inner mitochondrial membrane. *J. Biol. Chem.* **277,** 43553–43556 CrossRef Medline
7. Schlame, M., Rua, D., and Greenberg, M. L. (2000) The biosynthesis and functional role of cardiolipin. *Prog. Lipid Res.* **39,** 257–288 CrossRef Medline
8. Schlame, M., Acehan, D., Berno, B., Xu, Y., Valvo, S., Ren, M., Stokes, D. L., and Epand, R. M. (2012) The physical state of lipid substrates provides transacylation specificity for tafazzin. *Nat. Chem. Biol.* **8,** 862–869 CrossRef Medline
9. Schlame, M. (2008) Cardiolipin synthesis for the assembly of bacterial and mitochondrial membranes. *J. Lipid Res.* **49,** 1607–1620 CrossRef Medline
10. Xu, Y., Phoon, C. K., Berno, B., D'Souza, K., Hoedt, E., Zhang, G., Neubert, T. A., Epand, R. M., Ren, M., and Schlame, M. (2016) Loss of protein association causes cardiolipin degradation in Barth syndrome. *Nat. Chem. Biol.* **12,** 641–647 CrossRef Medline
11. Schlame, M., Kelley, R. I., Feigenbaum, A., Towbin, J. A., Heerdt, P. M., Schieble, T., Wanders, R. J., DiMauro, S., and Blanck, T. J. (2003) Phospholipid abnormalities in children with Barth syndrome. *J. Am. Coll. Cardiol.* **42,** 1994–1999 CrossRef Medline
12. Valianpour, F., Mitsakos, V., Schlemmer, D., Towbin, J. A., Taylor, J. M., Ekert, P. G., Thorburn, D. R., Munnich, A., Wanders, R. J., Barth, P. G., and Vaz, F. M. (2005) Monolysocardiolipins accumulate in Barth syndrome but do not lead to enhanced apoptosis. *J. Lipid Res.* **46,** 1182–1195 CrossRef Medline
13. Xu, Y., Sutachan, J. J., Plesken, H., Kelley, R. I., and Schlame, M. (2005) Characterization of lymphoblast mitochondria from patients with Barth syndrome. *Lab. Invest.* **85,** 823–830 CrossRef Medline
14. McKenzie, M., Lazarou, M., Thorburn, D. R., and Ryan, M. T. (2006) Mitochondrial respiratory chain supercomplexes are destabilized in Barth syndrome patients. *J. Mol. Biol.* **361,** 462–469 CrossRef Medline
15. Acehan, D., Xu, Y., Stokes, D. L., and Schlame, M. (2007) Comparison of lymphoblast mitochondria from normal subjects and patients with Barth syndrome using electron microscopic tomography. *Lab. Invest.* **87,** 40–48 CrossRef Medline
16. Gonzalvez, F., D'Aurelio, M., Boutant, M., Moustapha, A., Puech, J. P., Landes, T., Arnauné-Pelloquin, L., Vial, G., Taleux, N., Slomianny, C., Wanders, R. J., Houtkooper, R. H., Bellenguer, P., Møller, I. M., Gottlieb, E., *et al.* (2013) Barth syndrome: cellular compensation of mitochondrial dysfunction and apoptosis inhibition due to changes in cardiolipin remodeling linked to tafazzin (TAZ) gene mutation. *Biochim. Biophys. Acta* **1832,** 1194–1206 CrossRef Medline
17. Barth, P. G., Van den Bogert, C., Bolhuis, P. A., Scholte, H. R., van Gennip, A. H., Schutgens, R. B., and Ketel, A. G. (1996) X-linked cardioskeletal myopathy and neutropenia (Barth syndrome): respiratory-chain abnormalities in cultured fibroblasts. *J. Inherit. Metab. Dis.* **19,** 157–160 CrossRef Medline
18. Wang, G., McCain, M. L., Yang, L., He, A., Pasqualini, F. S., Agarwal, A., Yuan, H., Jiang, D., Zhang, D., Zangi, L., Geva, J., Roberts, A. E., Ma, Q., Ding, J., Chen, J., *et al.* (2014) Modeling the mitochondrial cardiomyopathy

of Barth syndrome with induced pluripotent stem cell and heart-on-chip technologies. *Nat. Med.* **20,** 616–623 CrossRef Medline
19. Dudek, J., Cheng, I. F., Balleininger, M., Vaz, F. M., Streckfuss-Bömeke, K., Hübscher, D., Vukotic, M., Wanders, R. J., Rehling, P., and Guan, K. (2013) Cardiolipin deficiency affects respiratory chain function and organization in an induced pluripotent stem cell model of Barth syndrome. *Stem Cell Res.* **11,** 806–819 CrossRef Medline
20. Huang, Y., Powers, C., Madala, S. K., Greis, K. D., Haffey, W. D., Towbin, J. A., Purevjav, E., Javadov, S., Strauss, A. W., and Khuchua, Z. (2015) Cardiac metabolic pathways affected in the mouse model of barth syndrome. *PLoS One* **10,** e0128561 CrossRef Medline
21. Dudek, J., Cheng, I.-F., Chowdhury, A., Wozny, K., Balleininger, M., Reinhold, R., Grunau, S., Callegari, S., Toischer, K., Wanders, R. J., Hasenfuë, G., Brügger, B., Guan, K., and Rehling, P. (2016) Cardiac-specific succinate dehydrogenase deficiency in Barth syndrome. *EMBO Mol. Med.* **8,** 139–154 CrossRef Medline
22. Kiebish, M. A., Yang, K., Liu, X., Mancuso, D. J., Guan, S., Zhao, Z., Sims, H. F., Cerqua, R., Cade, W. T., Han, X., and Gross, R. W. (2013) Dysfunctional cardiac mitochondrial bioenergetic, lipidomic, and signaling in a murine model of Barth syndrome. *J. Lipid Res.* **54,** 1312–1325 CrossRef Medline
23. Roberts, A. E., Nixon, C., Steward, C. G., Gauvreau, K., Maisenbacher, M., Fletcher, M., Geva, J., Byrne, B. J., and Spencer, C. T. (2012) The Barth Syndrome Registry: distinguishing disease characteristics and growth data from a longitudinal study. *Am. J. Med. Genet. A* **158A,** 2726–2732 CrossRef Medline
24. Acehan, D., Vaz, F., Houtkooper, R. H., James, J., Moore, V., Tokunaga, C., Kulik, W., Wansapura, J., Toth, M. J., Strauss, A., and Khuchua, Z. (2011) Cardiac and skeletal muscle defects in a mouse model of human Barth syndrome. *J. Biol. Chem.* **286,** 899–908 CrossRef Medline
25. Soustek, M. S., Falk, D. J., Mah, C. S., Toth, M. J., Schlame, M., Lewin, A. S., and Byrne, B. J. (2011) Characterization of a transgenic short hairpin RNA-induced murine model of tafazzin deficiency. *Hum. Gene Ther.* **22,** 865–871 CrossRef Medline
26. Phoon, C. K., Acehan, D., Schlame, M., Stokes, D. L., Edelman-Novemsky, I., Yu, D., Xu, Y., Viswanathan, N., and Ren, M. (2012) Tafazzin knockdown in mice leads to a developmental cardiomyopathy with early diastolic dysfunction preceding myocardial noncompaction. *J. Am. Heart Assoc.* **1,** jah3-e000455 CrossRef Medline
27. Karkucinska-Wieckowska, A., Trubicka, J., Werner, B., Kokoszynska, K., Pajdowska, M., Pronicki, M., Czarnowska, E., Lebiedzinska, M., Sykut-Cegielska, J., Ziolkowska, L., Jaron, W., Dobrzanska, A., Ciara, E., Wieckowski, M. R., and Pronicka, E. (2013) Left ventricular noncompaction (LVNC) and low mitochondrial membrane potential are specific for Barth syndrome. *J. Inherit. Metab. Dis.* **36,** 929–937 CrossRef Medline
28. Powers, C., Huang, Y., Strauss, A., and Khuchua, Z. (2013) Diminished exercise capacity and mitochondrial bc_1 complex Deficiency in Tafazzin-knockdown mice. *Front. Physiol.* **4,** 74 CrossRef Medline
29. Moullan, N., Mouchiroud, L., Wang, X., Ryu, D., Williams, E. G., Mottis, A., Jovaisaite, V., Frochaux, M. V., Quiros, P. M., Deplancke, B., Houtkooper, R. H., and Auwerx, J. (2015) Tetracyclines disturb mitochondrial function across eukaryotic models: a call for caution in biomedical research. *Cell Rep.* **10,** 1681–1691 CrossRef Medline
30. Chatzispyrou, I. A., Guerrero-Castillo, S., Held, N. M., Ruiter, J. P. N., Denis, S. W., L, I. J., Wanders, R. J., van Weeghel, M., Ferdinandusse, S., Vaz, F. M., Brandt, U., and Houtkooper, R. H. (2018) Barth syndrome cells display widespread remodeling of mitochondrial complexes without affecting metabolic flux distribution. *Biochim. Biophys. Acta Mol. Basis Dis.* **1864,** 3650–3658 CrossRef Medline
31. Nielsen, T. T., Stottrup, N. B., Løfgren, B., and Bøtker, H. E. (2011) Metabolic fingerprint of ischaemic cardioprotection: importance of the malate–aspartate shuttle. *Cardiovasc. Res.* **91,** 382–391 CrossRef Medline
32. Zhu, J., Vinothkumar, K. R., and Hirst, J. (2016) Structure of mammalian respiratory complex I. *Nature* **536,** 354–358 CrossRef Medline
33. Fiedorczuk, K., Letts, J. A., Degliesposti, G., Kaszuba, K., Skehel, M., and Sazanov, L. A. (2016) Atomic structure of the entire mammalian mitochondrial complex I. *Nature* **538,** 406–410 CrossRef Medline
34. Ngo, J. K., Pomatto, L. C., and Davies, K. J. (2013) Upregulation of the mitochondrial Lon Protease allows adaptation to acute oxidative stress but dysregulation is associated with chronic stress, disease, and aging. *Redox Biol.* **1,** 258–264 CrossRef Medline
35. Svensson, L. T., Alexson, S. E., and Hiltunen, J. K. (1995) Very long chain and long chain acyl-CoA thioesterases in rat liver mitochondria. Identification, purification, characterization, and induction by peroxisome proliferators. *J. Biol. Chem.* **270,** 12177–12183 CrossRef Medline
36. Wei, J., Kang, H. W., and Cohen, D. E. (2009) Thioesterase superfamily member 2 (Them2)/acyl-CoA thioesterase 13 (Acot13): a homotetrameric hotdog fold thioesterase with selectivity for long-chain fatty acyl-CoAs. *Biochem. J.* **421,** 311–322 CrossRef Medline
37. Eaton, S., Bursby, T., Middleton, B., Pourfarzam, M., Mills, K., Johnson, A. W., and Bartlett, K. (2000) The mitochondrial trifunctional protein: centre of a β-oxidation metabolon? *Biochem. Soc. Trans.* **28,** 177–182 CrossRef Medline
38. Taylor, W. A., Mejia, E. M., Mitchell, R. W., Choy, P. C., Sparagna, G. C., and Hatch, G. M. (2012) Human trifunctional protein α links cardiolipin remodeling to β-oxidation. *PLoS One* **7,** e48628 CrossRef Medline
39. Wanders, R. J., Meijer, A. J., Groen, A. K., and Tager, J. M. (1983) Bicarbonate and the pathway of glutamate oxidation in isolated rat-liver mitochondria. *Eur. J. Biochem.* **133,** 245–254 CrossRef Medline
40. Tahiliani, A. G., and Neely, J. R. (1987) A transport system for coenzyme A in isolated rat heart mitochondria. *J. Biol. Chem.* **262,** 11607–11610 Medline
41. Schlame, M., Towbin, J. A., Heerdt, P. M., Jehle, R., DiMauro, S., and Blanck, T. J. (2002) Deficiency of tetralinoleoyl-cardiolipin in Barth syndrome. *Ann. Neurol.* **51,** 634–637 CrossRef Medline
42. Mejia, E. M., Cole, L. K., and Hatch, G. M. (2014) Cardiolipin metabolism and the role it plays in heart failure and mitochondrial supercomplex formation. *Cardiovasc. Hematol. Disord. Drug Targets* **14,** 98–106 CrossRef Medline
43. Sparagna, G. C., and Lesnefsky, E. J. (2009) Cardiolipin remodeling in the heart. *J. Cardiovasc. Pharmacol.* **53,** 290–301 CrossRef Medline
44. Yamaoka, S., Urade, R., and Kito, M. (1990) Cardiolipin molecular species in rat heart mitochondria are sensitive to essential fatty acid–deficient dietary lipids. *J. Nutr.* **120,** 415–421 CrossRef Medline
45. Sparagna, G. C., Chicco, A. J., Murphy, R. C., Bristow, M. R., Johnson, C. A., Rees, M. L., Maxey, M. L., McCune, S. A., and Moore, R. L. (2007) Loss of cardiac tetralinoleoyl cardiolipin in human and experimental heart failure. *J. Lipid Res.* **48,** 1559–1570 CrossRef Medline
46. Letellier, T., Malgat, M., Rossignol, R., and Mazat, J. P. (1998) Metabolic control analysis and mitochondrial pathologies. *Mol. Cell. Biochem.* **184,** 409–417 CrossRef Medline
47. Milenkovic, D., Blaza, J. N., Larsson, N. G., and Hirst, J. (2017) The enigma of the respiratory chain supercomplex. *Cell Metab.* **25,** 765–776 CrossRef Medline
48. He, Q., Harris, N., Ren, J., and Han, X. (2014) Mitochondria-targeted antioxidant prevents cardiac dysfunction induced by tafazzin gene knockdown in cardiac myocytes. *Oxid. Med. Cell Longev.* **2014,** 654198 CrossRef Medline
49. Lopaschuk, G. D., Ussher, J. R., Folmes, C. D., Jaswal, J. S., and Stanley, W. C. (2010) Myocardial fatty acid metabolism in health and disease. *Physiol. Rev.* **90,** 207–258 CrossRef Medline
50. Safer, B. (1975) The metabolic significance of the malate–aspartate cycle in heart. *Circ. Res.* **37,** 527–533 CrossRef Medline
51. Cade, W. T., Spencer, C. T., Reeds, D. N., Waggoner, A. D., O'Connor, R., Maisenbacher, M., Crowley, J. R., Byrne, B. J., and Peterson, L. R. (2013) Substrate metabolism during basal and hyperinsulinemic conditions in adolescents and young-adults with Barth syndrome. *J. Inherit. Metab. Dis.* **36,** 91–101 Medline
52. Yudkoff, M., Nelson, D., Daikhin, Y., and Erecińska, M. (1994) Tricarboxylic acid cycle in rat brain synaptosomes: fluxes and interactions with aspartate aminotransferase and malate/aspartate shuttle. *J. Biol. Chem.* **269,** 27414–27420 Medline
53. Brown, G. K. (2005) Congenital brain malformations in mitochondrial disease. *J. Inherit. Metab. Dis.* **28,** 393–401 CrossRef Medline

54. Cade, W. T., Bohnert, K. L., Peterson, L. R., Patterson, B. W., Bittel, A. J., Okunade, A. L., de Las Fuentes, L., Steger-May, K., Bashir, A., Schweitzer, G. G., Chacko, S. K., Wanders, R. J., Pacak, C. A., Byrne, B. J., and Reeds, D. N. (2019) Blunted fat oxidation upon submaximal exercise is partially compensated by enhanced glucose metabolism in children, adolescents, and young adults with Barth syndrome. *J. Inherit. Metab. Dis.* **42,** 480–493 CrossRef Medline
55. Li, Y., Lou, W., Raja, V., Denis, S., Yu, W., Schmidtke, M. W., Reynolds, C. A., Schlame, M., Houtkooper, R. H., and Greenberg, M. L. (2019) Cardiolipin-induced activation of pyruvate dehydrogenase links mitochondrial lipid biosynthesis to TCA cycle function. *J. Biol. Chem.* **294,** 11568–11578 CrossRef Medline
56. Mejia, E. M., Ibdah, J. A., Sparagna, G. C., and Hatch, G. M. (2015) Differential reduction in cardiac and liver monolysocardiolipin acyltransferase-1 and reduction in cardiac and liver tetralinoleoyl-cardiolipin in the α-subunit of trifunctional protein heterozygous knockout mice. *Biochem. J.* **471,** 123–129 CrossRef Medline
57. Ostman-Smith, I., Brown, G., Johnson, A., and Land, J. M. (1994) Dilated cardiomyopathy due to type II X-linked 3-methylglutaconic aciduria: successful treatment with pantothenic acid. *Br. Heart J.* **72,** 349–353 CrossRef Medline
58. Rugolotto, S., Prioli, M. D., Toniolo, D., Pellegrino, P., Catuogno, S., and Burlina, A. B. (2003) Long-term treatment of Barth syndrome with pantothenic acid: a retrospective study. *Mol. Genet. Metab.* **80,** 408–411 CrossRef Medline
59. Mulligan, C. M., Le, C. H., deMooy, A. B., Nelson, C. B., and Chicco, A. J. (2014) Inhibition of delta-6 desaturase reverses cardiolipin remodeling and prevents contractile dysfunction in the aged mouse heart without altering mitochondrial respiratory function. *J. Gerontol. A Biol. Sci. Med. Sci.* **69,** 799–809 CrossRef Medline
60. Chicco, A. J., Le, C. H., Gnaiger, E., Dreyer, H. C., Muyskens, J. B., D'Alessandro, A., Nemkov, T., Hocker, A. D., Prenni, J. E., Wolfe, L. M., Sindt, N. M., Lovering, A. T., Subudhi, A. W., and Roach, R. C. (2018) Adaptive remodeling of skeletal muscle energy metabolism in high-altitude hypoxia: lessons from AltitudeOmics. *J. Biol. Chem.* **293,** 6659–6671 CrossRef Medline
61. Sparagna, G. C., Johnson, C. A., McCune, S. A., Moore, R. L., and Murphy, R. C. (2005) Quantitation of cardiolipin molecular species in spontaneously hypertensive heart failure rats using electrospray ionization mass spectrometry. *J. Lipid Res.* **46,** 1196–1204 CrossRef Medline
62. Pesta, D., and Gnaiger, E. (2012) High-resolution respirometry: OXPHOS protocols for human cells and permeabilized fibers from small biopsies of human muscle. *Methods Mol. Biol.* **810,** 25–58 CrossRef Medline
63. Gnaiger, E. (2009) Capacity of oxidative phosphorylation in human skeletal muscle: new perspectives of mitochondrial physiology. *Int. J. Biochem. Cell Biol.* **41,** 1837–1845 CrossRef Medline
64. Starkov, A. A. (2010) Measurement of mitochondrial ROS production. *Methods Mol. Biol.* **648,** 245–255 CrossRef Medline
65. Krumschnabel, G., Fontana-Ayoub, M., Sumbalova, Z., Heidler, J., Gauper, K., Fasching, M., and Gnaiger, E. (2015) Simultaneous high-resolution measurement of mitochondrial respiration and hydrogen peroxide production. *Methods Mol. Biol.* **1264,** 245–261 CrossRef Medline
66. Palladino, A. A., Chen, J., Kallish, S., Stanley, C. A., and Bennett, M. J. (2012) Measurement of tissue acyl-CoAs using flow-injection tandem mass spectrometry: acyl-CoA profiles in short-chain fatty acid oxidation defects. *Mol. Genet. Metab.* **107,** 679–683 CrossRef Medline
67. Käll, L., Storey, J. D., MacCoss, M. J., and Noble, W. S. (2008) Assigning significance to peptides identified by tandem mass spectrometry using decoy databases. *J. Proteome Res.* **7,** 29–34 CrossRef Medline
68. Smith, C. A., Want, E. J., O'Maille, G., Abagyan, R., and Siuzdak, G. (2006) XCMS: processing mass spectrometry data for metabolite profiling using nonlinear peak alignment, matching, and identification. *Anal. Chem.* **78,** 779–787 CrossRef Medline
69. Stein, S. E. (1999) An integrated method for spectrum extraction and compound identification from gas chromatography/mass spectrometry data. *J. Am. Soc. Mass Spectrometry* **10,** 770–781 CrossRef